Korean J. Chem. Eng., 33(2), 623-628 (2016)
DOI: 10.1007/s11814-015-0173-0

pISSN: 0256-1115
eISSN: 1975-7220

Impact of seed loading ratio on the growth kinetics of mono-ammonium phosphate under isothermal batch crystallization

Bingwen Long, Haotian Yang, and Yigang Ding†

Hubei Key Lab of Novel Reactor & Green Chemical Technology,
Key Laboratory for Green Chemical Process of Ministry of Education,
Wuhan Institute of Technology, Wuhan 430074, China
(*Received 18 January 2015 • accepted 7 August 2015*)

Abstract−The effect of seed load ratio on the growth kinetics of Mono-ammonium phosphate (MAP) under isothermal batch crystallization was investigated quantitatively. A direct parameter estimation method was proposed and applied to extract the growth kinetic parameters from a simple crystallization model using our experimental solution concentration decline data. The method assured the globally best parameters to be obtained and was found less sensitive to experimental errors. The linear growth constants k_g and the growth order g were found to be in the range of 1,000-2,600 $\mu m \cdot min^{-1}$ and 0.93-1.12, respectively, for MAP crystallized at 40 °C. Both parameters decreased significantly with increase of seed load ratio and k_g even showed a strong linear decline trend. The effective crystallization time also decreased with the seed mass. The proposed methodology could be extended to study the effect of other operation variables such as temperature and initial supersaturation on the crystal growth rate.

Keywords: Mono-ammonium Phosphate, Crystallization Kinetics, Seeding Effect, Parameter Estimation, Optimization

INTRODUCTION

Crystallization is probably the most widely employed process to purify solid phase products with size ranging from nano-scale particles to biological macromolecules [1]. In addition to the purity of the final crystals, physical characteristics such as the mean size, crystal size distribution (CSD) and shape usually need to meet stringent specifications for better downstream processing and product applications. To achieve the desired crystal properties, the crystallization process should be carefully and effectively controlled. Yet, the fundamental properties of crystallization are less understood compared to other unit operations such as distillation, extraction and absorption, and optimal control of the major process variables of the crystallization is still a major challenge [2].

Batch crystallization is employed due to its high flexibility, simple configuration, less investment and process development [3,4]. It generally involves two competing processes of nucleation and crystal growth. The tradeoff between them decides the size and CSD of final products. In most cases, crystal growth is favored and nucleation is undesirable in order to obtain narrow distributed crystals with large size [5]. An effective resolution is to introduce "seed" crystals at the beginning of the crystallization, providing surface area for crystals to grow without having to rely upon nucleation [6-8]. However, the amount and size of the charging seeds are crucial as they define the growth rate of the crystals and their quality. Poor CSD may be obtained if bad seeding choice is made. However, the mechanism of seeding is not well understood and the optimal seeding policy is still in debate [7,9]. Nevertheless, a generally accepted criterion for seeded batch crystallization is to maximize the growth of seeds while minimizing the growth of newly nucleated crystals [7,9,10]. Therefore, seeding effect on the growth rate of batch crystallization remains an important issue for both industrial and academic community.

Mono-ammonium phosphate (MAP) is a commercially useful compound that is extensively used as phosphorus fertilizers, fire-prevention coating and dry powder for fire extinguisher. The MAP crystal has a well-defined shape of tetragonal prism in combination with a tetragonal bipyramid [11]. When crystallized from water by cooling, MAP has a rather high growth rate and is able to withstand a significant degree of supersaturation before nucleation occurs, so the MAP-water system is very suitable for growth rate study in seeded crystallization [11-14]. Mullin and Amatavivadhana [11] first directly measured the face growth rate of a single MAP seed crystal in an isothermal batch crystallizer and found the growth process was second-order with respect to the supersaturation. Utomo et al. [13] also conducted isothermal seeded batch crystallization experiments at 10 °C. Effects of supersaturation, seed loading amount and seed size were investigated and the results showed that the seed loading ratio had the most significant effect on the products' CSD profiles, and the growth order was found to be 1.4. Following that, we put the focus of this research on the quantitative investigation of the effect of seed loading ratio on the growth kinetics of MAP in series of isothermal seeded batch crystallization experiments. The seed loading ratio here is defined as the ratio of the mass of seeds loaded into crystallizer to the theoretical maximum yield of crystal mass [15]. The crystallization temperature was chosen as 40 °C as this is the practically adopted crystallization temperature in industrial. The average size of the seed crystals was controlled

†To whom correspondence should be addressed.
E-mail: dygzhangli@163.com

around 600 μm to allow the growth of larger size MAP crystals that is often favored in some applications. These experimental conditions were carefully chosen to ensure crystallization was performed within the metastable width zone so that crystal growth on seeds dominates and secondary nucleation is effectively restrained. This work provides essential kinetic information and thus helps to gain in-depth understanding for the crystallization of MAP.

MATERIALS AND METHODS

1. Materials

Mono-ammonium phosphate (MAP) of analytical grade was obtained from the China National Pharmaceutical Foreign Trade Co. and then purified by recrystallization from water. The purity of recrystallized MAP was found to be higher than >99% (mass) by measuring both the composition of ammonia and phosphorus pentoxide [16]. Seed crystals around 600 μm were prepared by sieving and their average size (D50) was measured by laser light scattering (Mastersizer 2000, Malvern) as 615.8 μm and the surface area per gram crystals was measured as 0.0112 m^2/g. Double distilled water was used as the solvent.

2. Seeded Isothermal Batch Crystallization

The crystallization unit is schematically shown in Fig. 1. A 380 cm^3 jacketed glass cell equipped with a motor-driven stirrer was employed as the batch crystallizer. The temperature inside crystallizer was measured with a 4-wire platinum resistance probe (Pt-100) with an accuracy of ±0.02 K. The temperature was controlled by circulating water from a PID controlled thermostat (DTY-15A, Beijing DeTianYou Co.). During all the runs, the suspension temperature variation never exceeded ±0.1 °C after the thermostat controller started to stabilize the temperature. Continuous stirring with a constant speed of 250±20 rpm was applied for all the experiments.

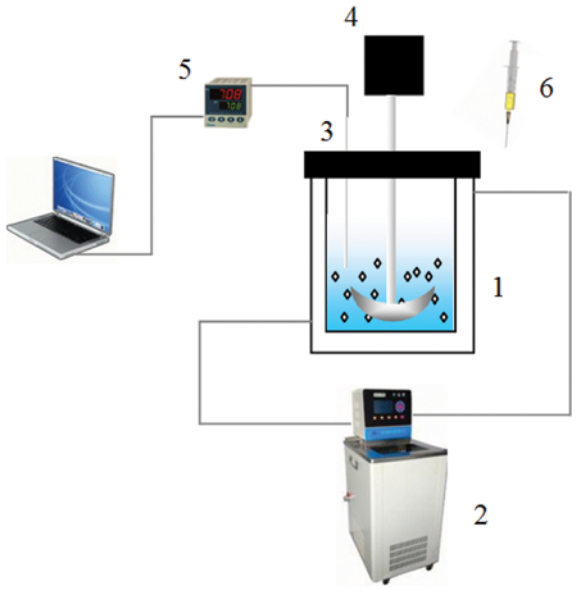

Fig. 1. Experiment set up.

1. Crystallizer
2. Thermostat
3. Pt-100 platinum resistance thermometer
4. Motor-driven stirrer
5. Temperature data acquisition unit
6. Syringe for sampling

Based on the reported solubility (0.5647 g/g H_2O) of MAP at 40 °C [17], supersaturated solutions of MAP were prepared by mixing certain amount of MAP crystals with water in the crystallizer. The mass of water was controlled around 200 g and accurately measured with an analytic balance for all the runs. The initial supersaturation was fixed as 0.05±0.002 g/g H_2O. The suspension was then heated to 45 °C and maintained for 30 min to get a clear solution. At the same time, a Yuguang AI-708 data acquisition unit collected the crystallization temperature data every 3 seconds from the Pt-100 probe, as described in our previous work [18]. After that, the solution was cooled to 40 °C and a sample for determination of the exact initial solution concentration was taken. No spontaneous nucleation was observed during the cooling process. When the temperature reached 40 °C, accurately weighed seed crystals of average size 615.8 μm were charged into the crystallizer. At intervals of 3 min for the first 20 min, clear solutions were withdrawn from the crystallizer for concentration analysis using a syringe fitted with a cotton filter at the tip, preventing the entrainment of solid crystals. To minimize the impact of sampling on the crystallization process, the amount of the samples was kept small (<1 mL). The total crystallization time was set as 120 min to allow full consumption of the supersaturation and thus the sufficient growth of the seed crystals.

The MAP concentration of the sample solution was determined by the gravimetric method [19-21], which had been successfully employed by Mullin to measure the solubility and supersaturation of MAP [11]. The balance used to measure the weight difference before and after solvent evaporation has an accuracy of ±0.1 mg. A series of six batch experiments with seed loads between 0.1 and 1.0 g was performed, corresponding to seed loading ratio between 0.01 and 0.1 as predefined. Since the solvent mass, crystallization temperature and initial supersaturation were almost identical for all the runs, we will directly use seed mass hereafter instead of seed loading ratio for the following discussion.

3. Crystallization Model

The material balance for the crystallizer is:

$$M=M_S+m_0(c_0-c) \tag{1}$$

where M and M_S are the mass of overall crystals and seeds, respectively; c is the solution concentration and c_0 is the initial solution concentration, which are both expressed as the solute mass per gram solvent, and therefore m_0 is the solvent mass which is assumed to be constant during the crystallization process.

On the kinetics of crystallization, M is proportional to the solution supersaturation Δc as [4]:

$$\frac{dM}{dt}=k_m A\left(\frac{c-c^*}{c^*}\right)^g \tag{2}$$

where k_m is the mass deposition rate constant and g is the growth order. Both parameters should be obtained by fitting the model to experimental data. At 40 °C, the equilibrium solubility of MAP in water, c^* is measured as 0.5651 g per gram water, which agrees well with the literature value of 0.5647 g per gram water [17]. Assuming constant crystal shape factors and negligible breakage and agglomeration, we can relate the total crystal surface area to the total crystal mass by the geometry similarity [4]:

$$A = A_S\left(\frac{M}{M_S}\right)^{2/3} \tag{3}$$

In which, the A_S and M_S denote the total surface area and mass of the seeds, respectively. By defining a dimensionless crystal mass $x=(M-M_S)/M_S$, Carbone et al. [22,23] substituted Eq. (2) and (3) into Eq. (1), and obtained an elegant expression that can easily separate the variables:

$$M_S\frac{dx}{dt} = k_m A_S\left(\frac{M_S}{c^* m_0}\right)^g (x+1)^{2/3}(x^*-x)^g \tag{4}$$

where x^* is the dimensionless crystal mass at equilibrium. Under the conditions of seeded isothermal batch crystallization, the term $A_S(M_S/c^*m_0)^g$ is constant. So, by integrating Eq. (4) using the initial condition x(0)=0, we get the governing equation of the crystallization process:

$$\frac{M_S}{A_S}\left(\frac{c^* m_0}{M_S}\right)^g \int_0^x \frac{dx}{(x+1)^{2/3}(x^*-x)^g} = k_m t \tag{5}$$

During each batch experiment, the MAP concentration versus time data were measured as exemplified in Fig. 2. The concentration data was first converted to dimensionless crystal mass x using the knowledge of seed mass and solvent mass. With a specified g value, the Left hand side (LHS) of Eq. (5) can be easily calculated by putting x data at different time into the upper limit of the integral term. Then a line without intercept should be obtained in a plot of LHS versus time and the slope gives k_m. To do that, however, the growth order g needs to be assumed first and a bad choice of g would give a very poor linear correlation of Eq. (5). So, optimal g could be selected within several candidates and k_m is determined accordingly. The computation is straightforward and simple to implement. But, if g is chosen manually, it will be time consuming on repeated numeric integrating and linear fitting to get a reasonable g. Moreover, only limited g values can be testified. Therefore, in this work, we optimize k_m and g simultaneously using the following objective function:

$$\text{Min } f(k_m, g) = \sum\left(\frac{M_S}{A_S}\left(\frac{c^* m_0}{M_S}\right)^g \int_0^x \frac{dx}{(x+1)^{2/3}(x^*-x)^g} - kt\right)^2 \tag{6}$$

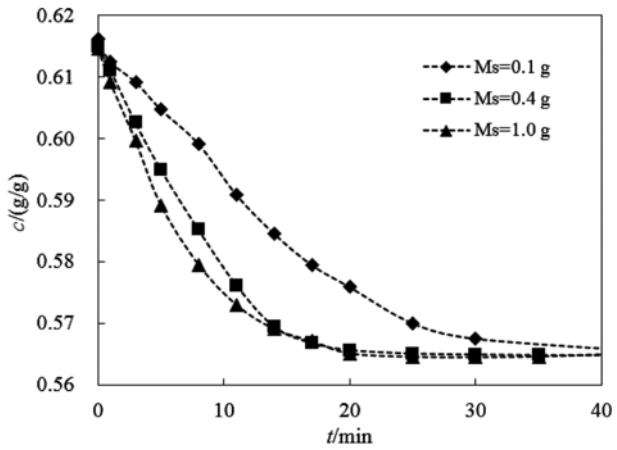

Fig. 2. Desupersaturation curves for batch crystallization experiments with different seed mass.

The computations were accomplished using Mathematica and the Levenberg-Marquardt algorithm is used for searching the best values of k_m and g.

RESULTS AND DISCUSSION

1. Desupersaturation Curves

A series of isothermal batch crystallization experiments with seed loading ratio between 0.01 and 0.1 was conducted. Desupersaturation curve was obtained by withdrawing clear solution periodically to determine the MAP concentration. Fig. 2 compares the desupersaturation curves obtained from crystallization experiments with different seed mass. Though all the crystallization experiments lasted for 120 min, the real supersaturation of the MAP solutions declined almost to zero when the operation time was over 40 min, as shown in the figure. Fig. 2 also indicates that the decline of MAP concentration speeds up as the seed mass increases, and this is more evident for the initial 20 min after seeds were charged. This is because the increase of the seed mass provides more surface areas for the solutes to deposit, and therefore results in faster consumption of the instant supersaturation. In addition, the MAP concentration directly declines almost linearly as soon as the crystallization starts, indicating the seed load amount was sufficient as to suppress the secondary nucleation and most of the supersaturation was consumed for the growth of seeds.

Table 1. Optimized growth kinetic parameters of MAP batch crystallization experiments with different seed loads

Seed mass (g)	k_m ($g\cdot m^{-2}\cdot min^{-1}$)	g	$R^{2,a}$	k_g ($\mu m\cdot min^{-1}$)
0.1	1120.67	1.10	0.9939	2572.68
0.2	1088.94	1.12	0.9977	2499.84
0.4	946.84	1.05	0.9990	2173.61
0.6	755.45	1.02	0.9989	1734.25
0.8	674.86	1.06	0.9978	1549.24
1.0	445.09	0.93	0.9923	1021.77

[a]R^2 is correlation coefficient of linear fit of Eq. (5)

Table 2. Example of MAP growth kinetics calculation through Eq. (1) to Eq. (5) with seed load of 0.40 g and solvent mass of 199.96 g

Time (min)	C (g/g H_2O)	M (g)	x	LHS of Eq. (5)
0	0.6149			
1	0.6111	1.1584	1.8961	2714.77
3	0.6025	2.8706	6.1764	6413.82
5	0.5949	4.3837	9.9593	9114.14
8	0.5851	6.3472	14.8680	12807.80
11	0.5761	8.1429	19.3573	17362.30
14	0.5694	9.4925	22.7314	23736.80
17	0.5667	10.0264	24.0661	29665.80
20	0.5656	10.2531	24.6326	35643.30
25	0.5650	10.3699	24.9246	44111.10
30	0.5649	10.4001	25.0003	50451.20
35	0.5648	10.4170	25.0425	60643.10

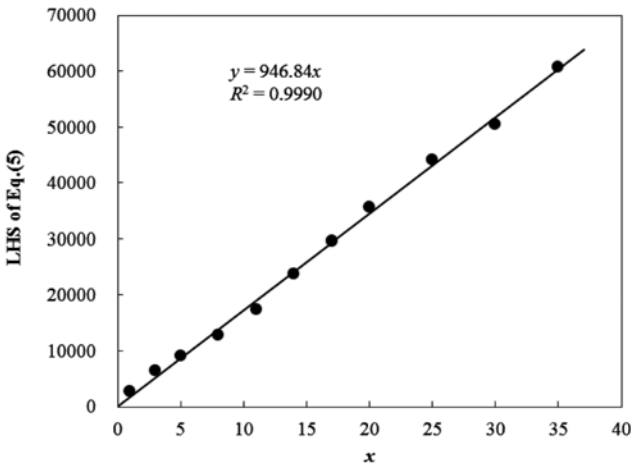

Fig. 3. Plots of Eq. (5) for batch crystallization with seed loading ratio of 0.04.

2. Determination of the Kinetic Parameters

The results of the optimized growth kinetic parameters are listed in Table 1. An example of data analysis using the pre-described model with detailed intermediate data is shown in Table 2. Fig. 3 was created using the first and last column data in the table. As expected, a strong linear relation is observed with an excellent correlation coefficient R^2 of 0.999. The linear correlation coefficients R^2 for other experiments are also listed in Table 1 and they are all higher than 0.99, indicating the applicability of Eq. (5) to our data.

3. Parameter Sensitivity Analysis

With the optimized growth kinetic parameters, we could reproduce the desupersaturation curve by solving Eq. (4). Eq. (4) is a first-order ordinary differential equation with the boundary condition x(0)=0. The built-in tool "NDSolve" in Mathematica was used to solve Eq. (5) numerically. The solution for seed mass of 0.4 gram is shown in Fig. 4 and good agreement is observed. We then tested the sensitivity of the growth kinetic parameters k_m and g by changing them for ±20% and ±10%, respectively. It can be seen from Fig. 4 that small changes of both parameters cause significant disagreement between the predicted and experimental desupersaturation curve. So, if g is assumed in prior and changed manually to search the optimal value by checking the goodness of fit of Eq. (5), the values to test are limited and the changing step is often not small enough. For example, Carbone [22,23] tested five *g* values between 1 and 3 with step size of 0.5 to determine the growth order of ovalbumin crystallization and found that g=2 gives better fit to experiment data in terms of correlation coefficient of Eq. (5) than the other four values and then claimed the growth order is 2. However, the best g is determined as 2.083 using proposed direct estimation method. In this work, the sensitivity of g for MAP solution was found less than 10%. With step change exceeding 50%, it is

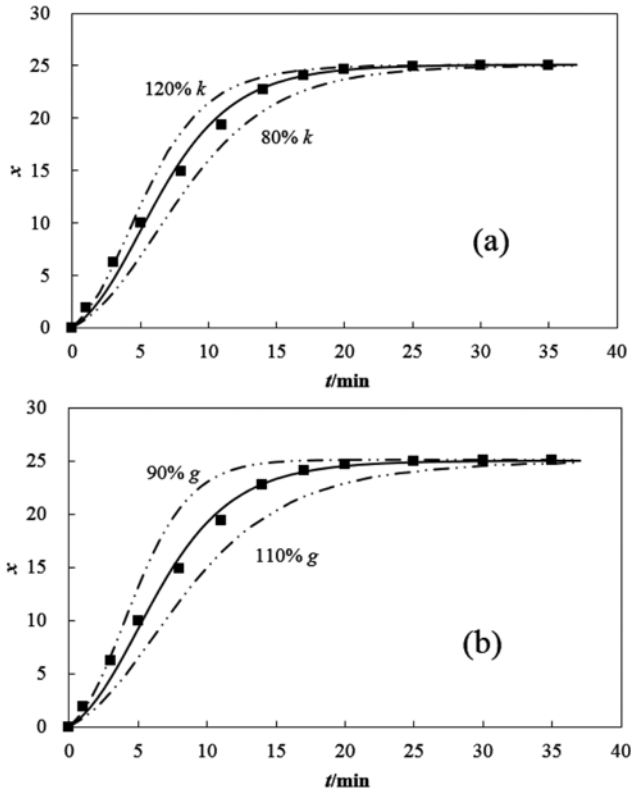

Fig. 4. Sensitivity of Eq. (4) to the optimized kinetic parameters. (a) Mass deposition rate constant k_m; (b) Growth order g.

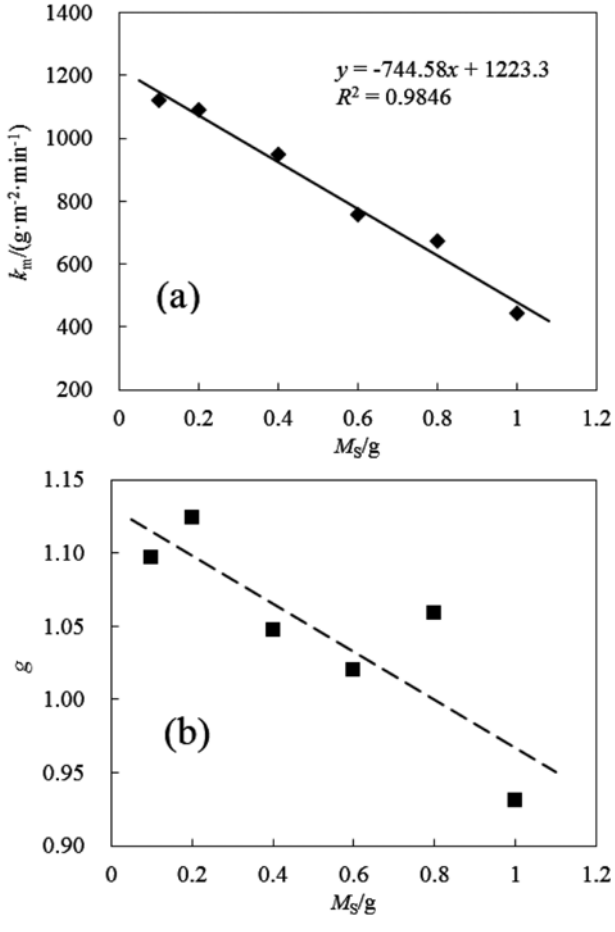

Fig. 5. The optimized kinetic parameters as function of seed mass. (a) Mass deposition rate constant k_m; (b) growth order g.

highly possible to miss the best g by manually tuning its value.

4. Effect of the Seed Crystal Mass

Fig. 5 presents plots of the optimized mass deposition rate constant k_m and growth order g versus seed mass. As can be seen, k_m shows rather high degree of linearity, which supports the constant crystal shape assumption for MAP and the validity of Eq. (3). The linear trend for g is not as clear as that for k_m, but it generally decreases with increasing seed mass. It is in the range of 0.9-1.15, comparable to the value of 1.4 as reported by Utomo et al. [13], who adopted the wavelet method to fit their supersaturation data. This difference may be attributed to the crystallization temperature and the parameter estimation method applied.

In literature, the linear growth rate, rather than the mass deposition rate is more often used to characterize the crystal growth kinetics. So, it is of interest to convert linear growth constant k_g from the mass deposition rate constants k_m. The linear growth rate is defined as [1]:

$$\frac{dL}{dt} = k_g\left(\frac{c-c^*}{c^*}\right)^g \tag{7}$$

where L is the characteristic length of the crystal, μm. Comparing Eq. (1) and Eq. (7), we get:

$$k_g = \frac{k_m A}{dM/dL} \tag{8}$$

and the mass and surface area of the crystals are:

$$M = \frac{\pi}{6} k_v \rho L^3 n_0 \tag{9}$$

$$A = k_a \pi L^2 n_0 \tag{10}$$

where k_v and k_a is the volume and surface area factor, respectively. n_0 is the number of crystals and ρ is the crystal density, which is 1.0803 g/cm^3 for MAP. Combining Eqs. (8), (9) and (10), we arrive at:

$$k_g = \frac{2k_a}{\rho k_v} k_m \tag{11}$$

The ratio of k_a/k_v can be obtained from geometric study of the seed crystals:

$$\frac{k_a}{k_v} = \rho \frac{A_S L_S}{M_S 6} \tag{12}$$

From our laser light scattering results, k_a/k_v is found to be 1.24 for MAP crystals. Then the linear growth constant, k_g, for each crystallization experiment are calculated from Eq. (11), and the results are also listed in Table 1. k_g is found to be in the range of 1,000-2,600 μm·min^{-1}, which falls well within literature k_g range of 2,300-2,900 μm·min^{-1} [13]. Following this, the linear growth rate along the desupersaturation curve can be estimated from Eq. (7). Fig. 6 shows the growth rate curves along the crystallization time for different seed mass loads. Lower growth rate is observed for crystallization experiments with high seed load ratio, which coincides with the desupersaturation curve results. This similarity implies that the addition of the seed load ratio would effectively increase the total surface areas available for the solute molecules to deposit and the crystals to grow and thus speed up the depletion of the instant supersaturation. So, as Eq. (7) tells, it is the supersaturation level in the solution that directly affects the growth rate. Note that the observation of decreased linear growth rate with seed load ratio in Fig. 6 is due to the kinetic parameters k_m and g both of which are found to be decrease with seed load ratio, so the linear growth rates calculated from Eq. (7) are indeed the overall linear growth rates, obtained based on the mass deposited per unit time per unit crystal surface area rather than on individual face growth rate [1]. Nevertheless, the intrinsic growth rate, according to the classic crystal growth theory, is related only to the properties of the individual crystal and the bulk properties of the solution. Therefore, the two kinetics parameters k_g and g should be theoretically independent on the operation variables such as the seed load ratio, cooling rate, etc., and this is true for many kinetic studies for single crystal growth where the intrinsic kinetics parameters for individual crystal are obtained. For industrial bulk solution crystallization, however, the mass transfer and the interactions between crystals and the solution and crystals of different size under different operation conditions are so complex that a simple power law equation like Eq. (7) is sometimes inadequate to describe all the cases. That is, it is still the supersaturation that manipulates the crystals' growth rate, but in our case it exerts its impact in a complex way that may not be fully represented by the simple power law, and the obtained kinetic parameters here are only the apparent rather than the intrinsic ones. Similar results have been reported by many studies [13,23-25], and Antonious [25] even found k_g was increasing with the seed mass by employing Eq. (7) to characterize the growth rate of barium chromate from water.

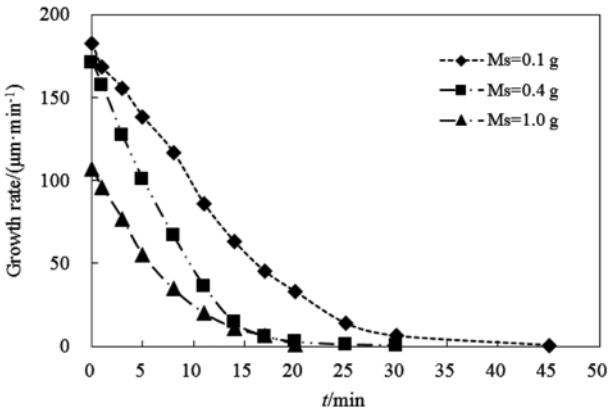

Fig. 6. Growth rate at different time for batch crystallization experiments with different seed mass.

In addition, it is found that the growth rate for seed mass greater than 0.4 g (seed loading ratio of 0.04) is actually close to zero at crystallization time around 20 min, while for seed mass of 0.1 g, it takes more than 40 min for the growth rate to decline to zero. Therefore, the proposed methodology can be practically used to predict the optimal crystallization time as a function of seed mass [22].

CONCLUSIONS

We have conducted a series of isothermal batch crystallization

experiments to study the growth kinetics of mono-ammonium phosphate crystallized from water. The experiments are designed to investigate the effect of seed crystal mass on the crystal growth rate. Desupersaturation curves for each experiment were obtained and used to extract the kinetic parameters of mass deposition rate constant and growth order. A direct estimation technique was proposed to optimize both kinetic parameters simultaneously. The results showed that the increases of seed crystal mass decreased both kinetic parameters. The growth order was in the range of 0.9-1.2 and the mass deposition rate constant showed good linear relation with seed crystal mass. The linear growth constants were then estimated and found to be in the range of 1,000-2,600 $\mu m \cdot min^{-1}$ and agreed well with the range reported in the literature. Low linear growth rate was observed for high seed load ratio crystallization experiment because the supersaturation is depleted more quickly on additional seeds' surface area. The effective crystallization time also decreased with the seed mass and 40 min was enough to deplete the initial supersaturation prepared in this work. The findings of present study allow the seeding methodology for crystallization of MAP to be controlled so as to yield a product with a desirable size within a reasonable crystallization time.

ACKNOWLEDGEMENTS

The authors thank the financial support from Key Technology R&D Program of Hubei Province (No. 2014BCB032), R&D Program of Low grade phosphate rock resources development and utilization Collaborative Innovation Center of Hubei Province (P201102) and the National Natural Science Foundation of China (No. 21303127).

REFERENCES

1. J. W. Mullin, *Crystallization*, 4th Ed., Butterworth-Heinemann, Oxford (2001).
2. L. A. Cisternas, C. M. Vásquez and R. E. Swaney, *AIChE J.*, **52**, 1754 (2006).
3. N. S. Tavare, J. Garside and M. R. Chivate, *Ind. Eng. Chem. Proc. Des. Dev.*, **19**, 653 (1980).
4. N. S. Tavare, *Chem. Eng. Comm.*, **61**, 259 (1987).
5. H. Hojjati and S. Rohani, *Chem. Eng. Process.*, **44**, 949 (2005).
6. N. Kubota, N. Doki, M. Yokota and A. Sato, *Powder Technol.*, **121**, 31 (2001).
7. C.-W. Hsu and J. D. Ward, *AIChE J.*, **59**, 390 (2013).
8. D. Kim and D. Yang, *Korean J. Chem. Eng.*, **32**, 1 (2015).
9. J. D. Ward, D. A. Mellichamp and M. F. Doherty, *AIChE J.*, **52**, 2046 (2006).
10. D. Kim, M. Paul, J.-U. Rapke, G. Wozny and D. Yang, *Korean J. Chem. Eng.*, **26**, 1220 (2009).
11. J. W. Mullin and A. Amatavivadhana, *J. Appl. Chem.*, **17**, 151 (1967).
12. J. W. Mullin, A. Amatavivadhana and M. Chakraborty, *J. Appl. Chem.*, **20**, 153 (1970).
13. J. Utomo, N. Maynard, Y. Asakuma, K. Maeda, K. Fukui and M. O. Tadé, *Adv. Powder Technol.*, **21**, 392 (2010).
14. J. Utomo, Y. Asakuma, N. Maynard, K. Maeda, K. Fukui and M. O. Tadé, *Chem. Eng. J.*, **156**, 594 (2010).
15. D. Jagadesh, N. Kubota, M. Yokota, N. Doki and A. Sato, *J. Chem. Eng. Jpn.*, **32**, 514 (1999).
16. G. H. Buchanan and G. B. Winner, *Ind. Eng. Chem.*, **12**, 448 (1920).
17. J. Eysseltova and T. P. I. Dirkse, *J. Phys. Chem. Ref. Data*, **27**, 1290 (1998).
18. B. Long, *Ind. Eng. Chem. Res.*, **50**, 7019 (2011).
19. B. Long, J. Li, R. Zhang and L. Wan, *Fluid Phase Equilib.*, **297**, 113 (2010).
20. B. Long and Z. Yang, *Fluid Phase Equilib.*, **266**, 38 (2008).
21. B. Long, J. Li, Y. Song and J. Du, *Ind. Eng. Chem. Res.*, **50**, 8354 (2011).
22. M. N. Carbone, R. A. Judge and M. R. Etzel, *Biotechnol. Bioeng.*, **91**, 84 (2005).
23. M. N. Carbone and M. R. Etzel, *Biotechnol. Bioeng.*, **93**, 1221 (2006).
24. H. A. Mohameed, B. Abu-Jdayil and M. A. Khateeb, *Chem. Eng. Process.*, **41**, 297 (2002).
25. M. S. Antonious, M. N. Ramsis and A. O. Youssef, *Monatsh. Chem.*, **127**, 15 (1996).